Journal of Molecular Liquids 437 (2025) 128613

Contents lists available at ScienceDirect

Journal of Molecular Liquids

journal homepage: www.elsevier.com/locate/molliq

Chemically surface-etched nanoparticles for tailored Pickering emulsions in enhanced oil recovery

Reza Khoramian [a], Kamila Ganiyeva [b], Miras Issakhov [c], Peyman Pourafshary [a,*], Saule Aidarova [c], Altynay Sharipova [d]

[a] School of Mining and Geosciences, Nazarbayev University, Astana, Kazakhstan
[b] Chemistry Department, Nazarbayev University, Astana, Kazakhstan
[c] Kazakh-British Technical University, Almaty, Kazakhstan
[d] Satbayev University, Almaty, Kazakhstan

ARTICLE INFO

Keywords:
Surface-etched silica nanoparticles
Pickering emulsions
Enhanced oil recovery
Emulsion stability
Disjoining pressure
Nanoparticles surface modification

ABSTRACT

Nanoparticles are widely used in Pickering emulsions, but their hydrophilic nature often limits interfacial effectiveness. This study explores a novel chemical etching method using the strong reductant sodium borohydride ($NaBH_4$) to enhance the interfacial properties of silica nanoparticles, improving oil recovery through more efficient Pickering emulsification. Characterization confirms surface etching through TEM and XPS, showing a rougher surface and a hydrodynamic size of 164.43 nm for etched silica, compared to 197.74 nm for bare silica. The etched silica nanoparticles exhibit increased hydrophobicity, as evidenced by FT-IR and contact angle measurements ($\theta = 75 \pm 1^\circ$ for etched silica vs. $\theta = 20 \pm 1^\circ$ for bare silica). At 500 ppm, modified silica nanoparticles facilitate Winsor emulsions I and II, with etched silica producing smaller, more stable droplets. Increasing the concentration to 2500 ppm reduces droplet size and tightens distributions, especially with etched silica, enhancing emulsion stability due to stronger interfacial layers, non-spherical shape, and lower bending resistance, as shown by desorption energy values of $\sim 3.91 \times 10^{-18}$ J for bare silica and $\sim 3.49 \times 10^{-16}$ J for etched silica. Pore-scale experiments demonstrate that surface-etched silica nanoparticles improve oil displacement and reduce residual trapping by promoting oil-in-water emulsions, outperforming bare silica due to stronger mechanical interactions, higher negative charge, and increased disjoining pressure (-4.81×10^{-4} Pa vs -8.38×10^{-4} Pa). This innovative modification approach, previously unexplored in oil recovery, offers a new pathway for enhanced oil mobilization and emulsion stability, with potential for broader applications in wastewater treatment, catalysis, and pharmaceuticals.

1. Introduction

Nanoparticles are widely used as stabilizers for Pickering emulsions, where they adsorb at the oil-water interface to prevent droplet coalescence [1]. However, bare hydrophilic nanoparticles often lack strong adsorption at the interface, limiting their effectiveness in stabilizing emulsions [2]. To improve stability, nanoparticles must be made partially hydrophobic to enhance their interfacial affinity [3]. Various surface engineering techniques have been developed to tailor the wettability of nanoparticles, optimizing their performance in emulsification processes [4]. These methods modify the surface properties, such as energy, charge, and chemistry, enabling nanoparticles to more effectively stabilize oil-in-water emulsions and facilitate enhanced oil recovery (EOR) applications [5].

One commonly used surface modification technique is silanization, where alkoxysilanes react with hydroxyl groups on the nanoparticle surface to introduce hydrophobic functional groups [6]. For instance, Lee et al. [7] modified $CaCO_3$ nanoparticles with methyltrimethoxysilane, a silane coupling agent, enhancing emulsion stability in oil-water systems by increasing surface hydrophobicity and making them strong candidates for emulsification applications. Maaref et al. [8] synthesized silica nanoparticles from sodium silicate and silanized them with hexamethyldisilazane, replacing surface silanol groups with hydrophobic trimethylsilyl groups to make them capable to adjust wettability. The modified nanoparticles effectively stabilized emulsions, as demonstrated by high zeta potential and improved surface coverage,

* Corresponding author.
E-mail address: peyman.pourafshary@nu.edu.kz (P. Pourafshary).

https://doi.org/10.1016/j.molliq.2025.128613
Received 23 April 2025; Received in revised form 7 September 2025; Accepted 24 September 2025
Available online 26 September 2025
0167-7322/© 2025 Elsevier B.V. All rights are reserved, including those for text and data mining, AI training, and similar technologies.

proving their suitability for oil recovery purposes [9]. Similarly, Alkotzer et al. [10] developed oil-in-water Pickering emulsions by in situ functionalization of hydrophilic silica nanoparticles with dodecyltriethoxysilane and 3-(aminopropyl) triethoxysilane. This modification enhanced emulsion stability and homogeneity by forming polysiloxane networks as solid shells around the droplets.

Another surface modification method is polymer grafting [11], where hydrophobic or amphiphilic polymers are covalently attached to nanoparticle surfaces [12]. Kaiser et al. [13] developed magneto-responsive Pickering emulsions stabilized by polystyrene-coated magnetic iron oxide nanoparticles with varying shell thicknesses. The stability of the emulsion was attributed to the "brick-and-mortar" structure formed by the entanglement of polymer shells at the oil–water interface. Similarly, Gholinezhad et al. [14] produced smaller, more uniform, and stable oil-in-water droplets using covalently ethylene glycol-coated silica nanoparticles. Qi et al. [15] synthesized pH-responsive silica nanoparticles by grafting poly (2-(dimethylamino) ethyl methacrylate) chains via a grafting-through technique. The polymer-coated silica nanoparticles stabilized heavy oil-in-water emulsions at 0.1 wt% and neutral pH. The emulsions exhibited high stability due to the irreversible adsorption of nanoparticles at the oil–water interface, with destabilization occurring at lower acidic pH.

Coating with surfactants is another widely used approach for modifying nanoparticles [16]. Surfactants adsorb onto the nanoparticle surface, altering their wettability, surface charges, and interfacial properties. Zhu et al. [17] used ionic surfactants to modify the surface of silica nanoparticles, creating switchable Pickering emulsions. Destabilization occurred by adding anionic surfactant, and restabilization was achieved by reintroducing cationic surfactant. Khoramian et al. [2] demonstrated that coating graphene oxide nanosheets with sodium dodecylbenzene sulfonate significantly enhanced their emulsifying ability in oil-in-water systems, surpassing the performance of silica nanoparticles. Wei et al. [18] altered the surface of nanoparticles from hydrophilic to hydrophobic using various cationic surfactants. These surfactants enhanced the stability of oil-in-water Pickering emulsions, exhibiting excellent salt tolerance and acid-base resistance due to strong surfactant adsorption on the nanoparticle surface, as confirmed by zeta potential and contact angle measurements.

Another modification technique is surface oxidation [19], a key process used to alter the surface of carbon-based nanoparticles, including graphene [20] and carbon nanotubes [21], to enhance their dispersibility in water. Khoramian et al. [22] oxidized graphene flakes' surface by adding oxygen-containing groups through chemical reactions, followed by post-synthesis probe ultrasonication to break down large flakes into smaller ones. This process facilitated the formation of toluene-in-water Pickering emulsions with droplet sizes below 10 μm. Similarly, Kim et al. [23] demonstrated that graphene oxide, with its amphiphilic nature, hydrophilic edges and a relatively hydrophobic basal plane, acts as a colloidal surfactant. They successfully created highly stable Pickering emulsions of organic solvents like toluene in water, forming submillimetre-sized droplets that remained stable for months due to graphene oxide's high surface area, which enabled kinetic trapping at the interface and prevented coalescence. Chen et al. [24] also formed stable water-in-oil emulsions with crude oil using 50–100 ppm graphene oxide, achieving an emulsion viscosity of 100–200 cP at a fixed shear rate of 7.34 s^{-1} over time. This stability was attributed to the unique structure of graphene oxide—1 nm thickness and surface functional groups such as Hydroxyl group (−OH), Carboxyl group (−COOH), Epoxy group (C—O), Carbonyl group (C═O), and Ether group (C-O-C).

One less explored but promising method is surface etching, which physically alters the surface morphology of nanoparticles by creating rougher, more porous surfaces. Through selective stripping of surface atoms or layers via chemical processes, this method enables precise control over the shape, surface chemistry, and size of nanoparticles, offering opportunities to enhance interfacial properties and activities. Surface etching has been studied for various applications. For instance, Zhang et al. [25] introduced an encapsulation and etching method to form porous silica shells around metal nanoparticles using NaOH, enhancing mass transfer while preventing aggregation. This approach improved catalytic stability and recyclability in both liquid- and gas-phase reactions. Similarly, Du and He [26] developed a self-templated etching strategy using $NaBH_4$ to transform smooth SiO_2 nanospheres into rough silica nanoparticles. By controlling the reaction time, they tailored smaller surface particles and produced superhydrophobic glass coatings with dual-size roughness after calcination and hydrophobic modification. Ahmadi et al. [27] investigated polymer-coated magnetic nanoparticles with varying polymer-to-core ratios (4:1, 3:1, 2:1, 1:1, and 0.5:1), which altered particle surface thickness and enabled the stabilization of oil-in-water Pickering nanoemulsions, thereby improving transport efficiency in porous media. However, systematic evaluation of surface-etched silica nanoparticles and their role in crude-oil/water emulsification remains comparatively limited, and this study addresses that gap. In this study, we engineer the surface chemistry and size of silica nanoparticles using sodium borohydride and polymer treatments to enhance their hydrophobicity. These modifications not only optimize emulsification performance and stability in Pickering emulsions but also improve pore-scale oil recovery by altering wettability and interfacial interactions, facilitating the efficient displacement of trapped oil. Our findings offer important perspectives on nanoparticle design for advanced energy applications, specifically in EOR.

2. Experimental methodology

2.1. Materials

Polyvinylpyrrolidone (PVP), a water-soluble, non-ionic polymer, was obtained from Sigma-Aldrich (Germany). In this study, PVP served as a dispersant and surface modifier to prevent complete etching of silica nanoparticles and to impart partial hydrophobic character to their surfaces. Silica nanoparticles (99.9 % purity) in nanopowder form were supplied by Thermo Fisher Scientific Chemicals (USA). Sodium borohydride ($NaBH_4$, 98 % purity) was also procured from Thermo Fisher Scientific Chemicals, and ethanol was sourced from Sigma-Aldrich. Sodium hydroxide (NaOH) pellets were purchased from Sigma-Aldrich, while hydrochloric acid (HCl) was obtained from Prakash Chemicals International, India. The crude oil used in the experiments, obtained from an oil field in western Kazakhstan, had a viscosity of 5 cP and a density of 0.846 g/cm^3 at standard conditions, corresponding to a light-to-medium crude representative of conventional reservoirs in this region.

2.2. Synthesis of surface-etched silica nanoparticles

Powdered silica nanoparticles (1.5 g) were dispersed in 50 mL of distilled water (pH 6.5) using a magnetic stirrer at 500 rpm for 30 min, followed by 2000 rpm for another 30 min. The dispersion was then subjected to an ultrasonic homogenizer for four cycles of 15 min at 85 % power, with alternating 5-s on/off pulses to ensure uniform dispersion. Resting intervals between cycles prevented overheating. The initial magnetic stirring step served to achieve uniform wetting and pre-dispersion of the nanoparticles, thereby facilitating their subsequent breakdown by ultrasonication, which acted as the primary high-energy dispersion method. PVP (1.25 g) was added to the nanofluid, stirred, and treated with ultrasound under identical conditions. Then, $NaBH_4$ (3 g) was gradually introduced while stirring at 1000 rpm at 50 °C for five hours. As a strong reducing agent, $NaBH_4$ facilitated the etching process, generating heat and boiling bubbles. PVP was incorporated to regulate this reaction, preventing excessive etching and preserving the silica nanoparticles' structural integrity. The resulting suspension was transferred to a 50 mL plastic tube and centrifuged at 9500 rpm for 20 min. The supernatant was discarded, and the precipitate was dispersed in 50

mL of distilled water using a high-speed shaker. This washing and centrifugation cycle was repeated four times with water and three times with ethanol to remove unreacted materials. Finally, the purified nanoparticles were dried in an oven at 60 °C for 24 h, yielding surface-etched silica nanoparticles.

2.3. Characterization of surface-etched silica nanoparticles

The synthesized surface-etched silica nanoparticles were characterized using various analytical techniques to evaluate their structural, morphological, and surface properties, with bare silica serving as a reference. Fourier-transform infrared spectroscopy (FT-IR) (Nicolet iS10 FT-IR Spectrometer) was specifically employed to identify any new functional groups introduced during the etching process. This analysis aimed to detect carbon-based or other chemical groups that were absent in untreated silica but emerged in surface-modified silica, thereby confirming successful surface modification. Scanning electron microscopy (SEM) (ZEISS Crossbeam 540) was used to examine the morphology and particle size, while transmission electron microscopy (TEM) (JEOL JSM-IT200) provided a more detailed analysis of surface texture by utilizing electron transmission through the nanoparticles. For SEM and TEM analyses, a 100-ppm nanofluid was dried onto small grids before imaging.

X-ray photoelectron spectroscopy (XPS) (NEXSA G2 System, Thermo Scientific, USA) was performed to analyze surface composition and chemical states of the etched SiO_2 nanoparticles. High-resolution scans were conducted for Si2p to assess changes in silicon oxidation states, O1s to examine modifications in the oxygen bonding environment, C1s to confirm PVP attachment or contamination, and Na1s to detect residual sodium from $NaBH_4$ treatment. Atomic force microscopy (AFM) (LabRAM HR Evolution Omega Scope) was employed to assess surface roughness and quantify topographical changes induced by $NaBH_4$ etching. The analysis provided a roughness factor (r_f), comparing the actual surface area to the projected smooth surface area. An increase in r_f confirmed surface roughening, indicating that the etching process disrupted the silica structure by selectively breaking Si—O bonds. Dynamic light scattering (DLS) (PMX-230 ZetaView TWIN Laser) was used to measure the hydrodynamic size distribution of silica nanoparticles before and after etching, tracking changes in mean particle size and distribution width. Zeta potential measurements (PMX-230 ZetaView TWIN Laser) were performed to assess surface charge modifications, focusing on shifts in charge density following $NaBH_4$ treatment. A 10-ppm nanofluid was used for DLS measurements to ensure accurate size distribution and stability analysis.

2.4. Oil-in-water emulsion analysis

Oil-in-water Pickering emulsions were prepared using both treated and untreated silica nanoparticles. The preparation procedure involved the dropwise addition of 10 mL of crude oil into 15 mL of nanofluid contained in a transparent glass vial, over a period of 30 min through a syringe needle, while stirring at 2000 rpm with a magnetic stirrer. This corresponds to an oil-to-water ratio of 2:3, which was selected to ensure stable emulsion formation under the given mixing conditions. Emulsions were formulated at nanoparticle concentrations of 500, 1000, 1500, 2000, and 2500 ppm to examine their influence on emulsion stability and droplet size. A microscopic camera with a magnification of 1600× was used to capture microscopic images for size analysis, and the droplet size distribution was measured using ImageJ software to assess the impact of surface modification on emulsion characteristics. The obtained results were compared to evaluate differences in stability and size between treated and untreated nanoparticles.

2.5. Measurement of interfacial tension and contact angle

Two glass microscope slides were coated with untreated and etched silica nanofluids, dried at room temperature for 24 h, and used for contact angle experiments to evaluate wettability conditions. The coated glass slides were placed in a transparent cube cell filled with water, and an oil droplet was introduced from below onto the solid surfaces. The droplet shape was recorded using a microscope camera and analyzed to determine contact angles. Interfacial tension (IFT) between crude oil and each nanofluid was measured using an IFT-700 instrument from Vinci Technologies. The cell was filled with the respective nanofluid, and an oil droplet was introduced, suspended from a needle. The droplet shape was analyzed to quantify interfacial tension.

2.6. Pore-scale oil recovery study

A glass micromodel with a five-spot pattern, designed for visualizing fluid flow in reservoir rock samples [28], was fabricated by etching a glass plate (Fig. 1a) and fusing it to another glass plate (10 cm × 5 cm) at 700 °C. The micromodel, featuring inlet and outlet ports for fluid injection and production (Fig. 1b), was used to visualize nanofluid-assisted oil recovery at the pore scale. The experimental setup mainly consisted of a backlight, a syringe pump, and a microscope camera. The micromodel was initially saturated with crude oil to establish baseline conditions. Then, 1 pore volume of nanofluid was injected at a controlled rate of 0.01 cc/min, and the displacement process was recorded using a high-resolution microscope camera. The evolution of trapped and mobilized oil phases was analyzed to assess recovery efficiency. Two nanofluid formulations, untreated and surface-modified silica nanoparticles, were tested to evaluate their impact on dynamic in-situ emulsification and oil mobilization. Microscopic images were processed to quantify fluid distribution and determine the effectiveness of each formulation in enhancing oil displacement.

3. Results and discussions

3.1. Characterizations

Fig. 2a shows the FTIR spectra of bare SiO_2 nanoparticles (blue) and surface-etched SiO_2 nanoparticles (red), revealing key structural and chemical modifications induced by $NaBH_4$ etching in a distilled water-PVP mixture. The bare SiO_2 spectrum exhibits characteristic silica peaks, including a strong Si–O–Si asymmetric stretching vibration near 1100 cm^{-1} [29], a symmetric Si–O–Si stretching peak at 800 cm^{-1} [30], and a weak hydroxyl (–OH) peak around 3400 cm^{-1} [31], likely from adsorbed water. These features confirm the structural integrity of the unmodified silica nanoparticles. The surface-etched SiO_2 spectrum closely matches the bare SiO_2 spectrum, indicating the preservation of the silica framework. However, two notable differences, highlighted in cyan and purple, confirm surface modification. The purple-shaded region between 2750 and 3000 cm^{-1} corresponds to C—H stretching vibrations (–CH_2 and –CH_3 groups), indicating the introduction of hydrophobic functionalities onto the silica surface [32]. The cyan-shaded band around 1390 cm^{-1} is attributed to C—N stretching or CH_3 bending, arising from residual PVP polymer used during synthesis [33]. The FTIR findings are strongly supported by the high-resolution XPS C1s spectra (Figs. 2b–c). For the bare SiO_2 nanoparticles, the C1s signal shows a weak peak at 287.1 eV with an intensity of around 16,103.7 (a.u.), primarily assigned to C═O or C—N species from adventitious carbon. After etching, the etched sample exhibits a stronger and slightly shifted peak at 287.59 eV with an intensity of about 19,131.5 (a.u.), reflecting the enrichment of organic fragments such as PVP residues and newly introduced hydrocarbon groups. The shift toward higher binding energy suggests the presence of more electronegative C–N/C=O environments, while the increased intensity confirms higher carbon incorporation. This enhanced carbon signature is a clear marker of successful surface modification with $NaBH_4$ and PVP, which is expected to improve nanoparticle affinity for oil–water interfaces. (For interpretation of the references to colour in this figure legend, the reader

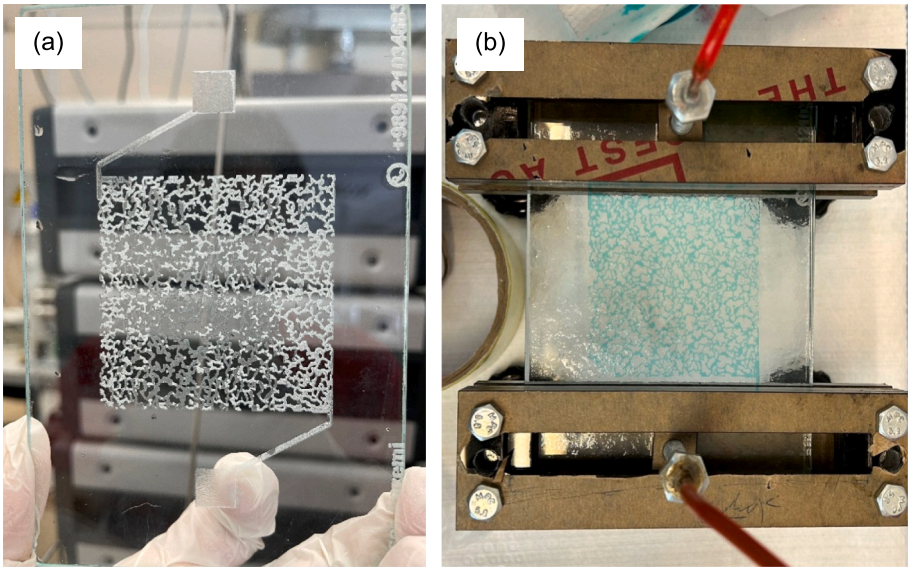


Fig. 1. (a) The etched glass plate with a five-spot pattern. (b) Fabricated glass micromodel after fusion, featuring inlet and outlet ports for fluid injection and production.

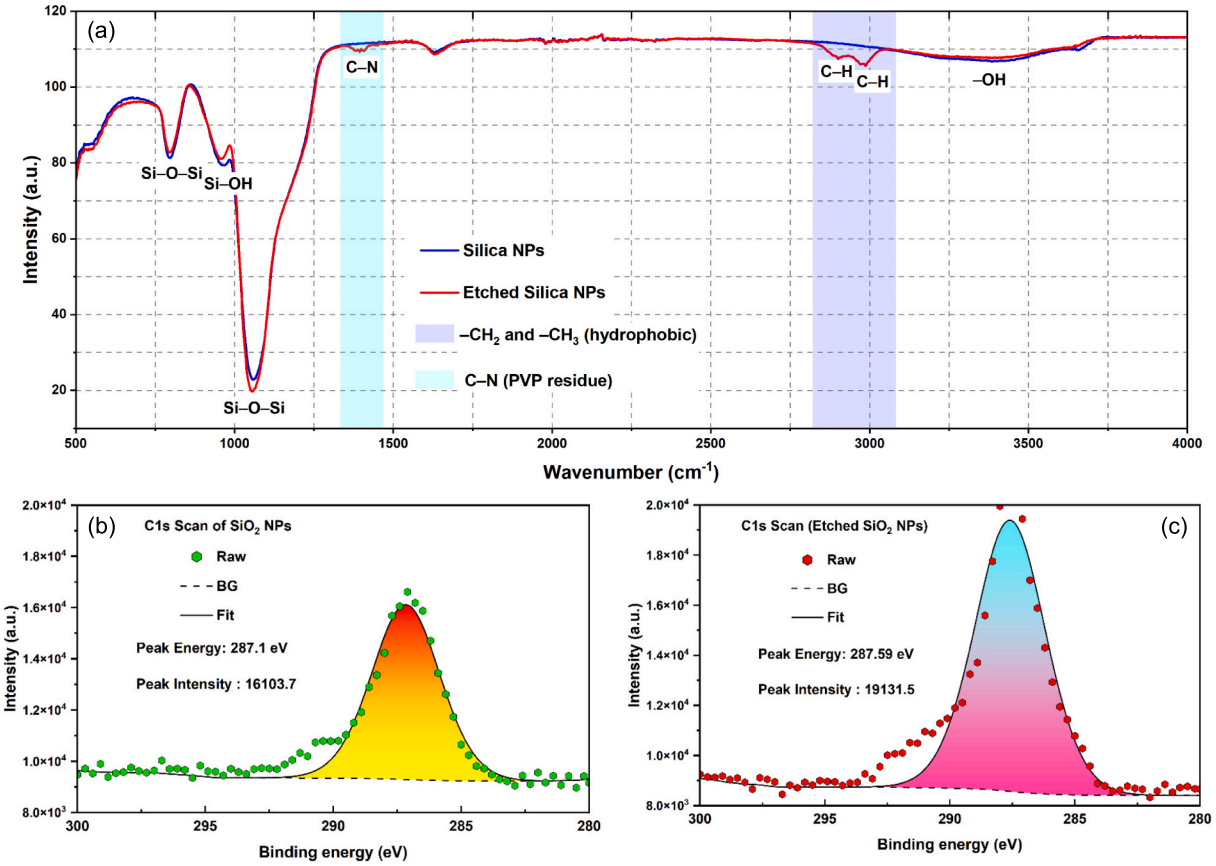


Fig. 2. (a) FTIR spectra of silica nanoparticles (NPs) before (blue) and after (red) etching. Peaks at 2750–3000 cm^{-1} (C—H stretching, $–CH_2/–CH_3$) indicate hydrophobic groups, while the band at 1390 cm^{-1} corresponds to C—N stretching from PVP residues. Shaded regions (purple: C—H, cyan: C—N) highlight the functional groups introduced after etching. (b) High-resolution XPS C1s spectrum of silica NPs, showing a peak at 287.1 eV. (c) High-resolution XPS C1s spectrum of etched silica NPs, with an increased peak intensity at 287.59 eV, indicating surface modification (*BG: background*). (For interpretation of the references to colour in this figure legend, the reader is referred to the web version of this article.)

is referred to the web version of this article.)

The SEM micrograph of bare SiO_2 nanoparticles (Fig. 3a) shows smooth, uniform surfaces with a well-defined spherical morphology. In contrast, the etched nanoparticles (Fig. 3b) exhibit a rougher surface texture, indicating successful modification, which likely enhances the surface area and charge. In addition, the nanoparticles tend to form

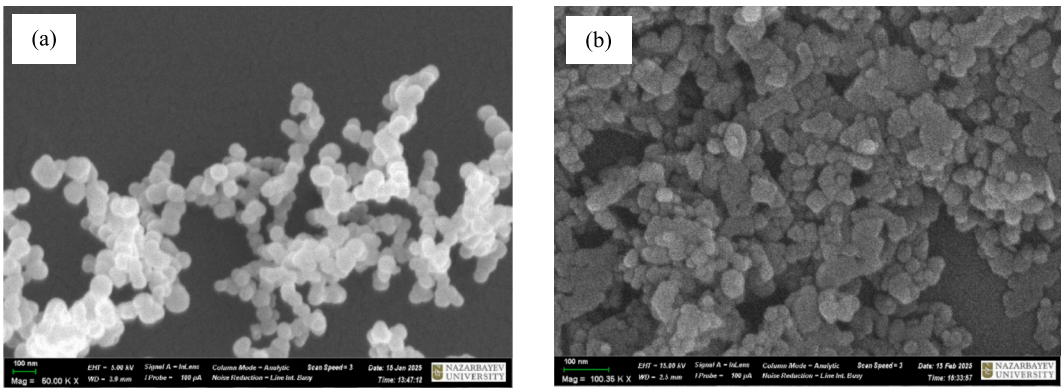


Fig. 3. SEM micrographs of SiO_2 nanoparticles: (a) bare nanoparticles; (b) surface-etched nanoparticles treated with $NaBH_4$.

clusters, consistent with the grape-like aggregates typical of precipitated silica (Fig. 4). This clustering behaviour arises from the intrinsic aggregation tendency of silica nanoparticles, further promoted by surface modifications during etching, and helps explain the differences in their interfacial behaviour.

TEM analysis was performed to further examine the morphology and surface characteristics of SiO_2 nanoparticles before and after surface etching with $NaBH_4$ (Fig. 5). The transmission of electrons through the nanoparticles provides detailed insight into surface modifications, revealing morphological changes induced by the etching process.

The bare silica nanoparticles (**Fig. 5a** and **c**) exhibit a smooth, uniform spherical structure with well-defined boundaries, as indicated by their consistent shape. The nanoparticles appear with minimal surface irregularities, confirming their high degree of uniformity. In contrast, the $NaBH_4$-treated nanoparticles (**Fig. 5b** and **d**) display surface roughening, characterized by non-uniform edges. The increased surface roughness was confirmed through AFM analysis. A dimensionless number, the roughness factor (r_f) [34], is defined as:

$$r_f = \frac{\text{actual surface area}}{\text{projected surface area}} \quad (1)$$

The actual surface area accounts for microscopic peaks, valleys, and texture, increasing with roughness. The projected surface area represents the particle's area if it were perfectly smooth, viewed from the top, approximating an idealized shape.

- If $r_f = 1$, the surface is smooth.
- If $r_f > 1$, the surface is rough, meaning the actual surface area is larger.

AFM analysis showed an increase in r_f from 1.035 to 1.264, confirming significant roughness enhancement. The actual and projected surface area values for both nanoparticles are reported in Table 1. This increase in roughness indicates that the chemical etching process with $NaBH_4$ likely disrupted the smooth morphology of the nanoparticles by removing surface atoms. This transformation can be attributed to the reducing nature of $NaBH_4$, which selectively etches silica surfaces by breaking Si—O bonds [35], leading to material loss during the etching process.

This morphological transformation is consistent with the Si2p XPS spectra (Figs. 6a–b). For the bare nanoparticles, the Si2p peak appears at 105.8 eV with an intensity of around 54,866.7 (a.u.), characteristic of Si^{4+} in the Si–O–Si lattice. After etching, the peak remains at 105.8 eV but decreases in intensity to about 46,422.9 (a.u.), indicating partial removal of surface silicon atoms and a reduction in the overall Si—O signal. The decrease in Si2p intensity thus directly supports AFM evidence of surface atom loss and roughening. In addition, the Na1s scans (Figs. 6c–d) show a marked increase in peak intensity from around 41,668.2 (a.u.) in bare silica to about 77,005.4 (a.u.) in etched silica, with a consistent binding energy near 1074 eV. This sharp increase demonstrates the incorporation of sodium species, most likely due to $NaBH_4$ interaction with surface silanols and the deposition of Na^+ ions. The combined decrease in Si2p intensity and rise in Na1s signal provide strong chemical evidence that $NaBH_4$ etching alters both the structural and chemical environment of the silica surface. Such modification enhances the availability of anchoring sites for interfacial interactions, improving the nanoparticles' potential performance in oil–water displacement processes.

Fig. 7a presents the particle size distribution analysis from DLS for untreated and surface-treated silica nanoparticles. The size distributions of etched silica (orange) and bare silica (blue) exhibit a similar overall trend, indicating a homogeneous pattern. However, the etched silica displays a more symmetric peak centred at 164.43 nm, with minimal presence of particles beyond 300 nm, suggesting that the etching process

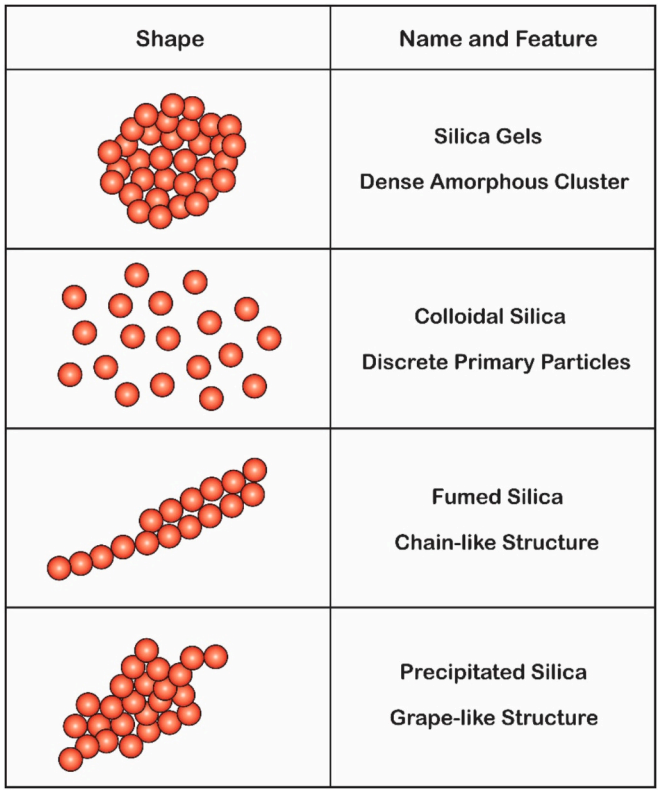


Fig. 4. Schematic classification of SiO_2 nanoparticles according to their morphology: silica gels (dense amorphous clusters), colloidal silica (discrete primary particles), fumed silica (chain-like structures), and precipitated silica (grape-like aggregates).

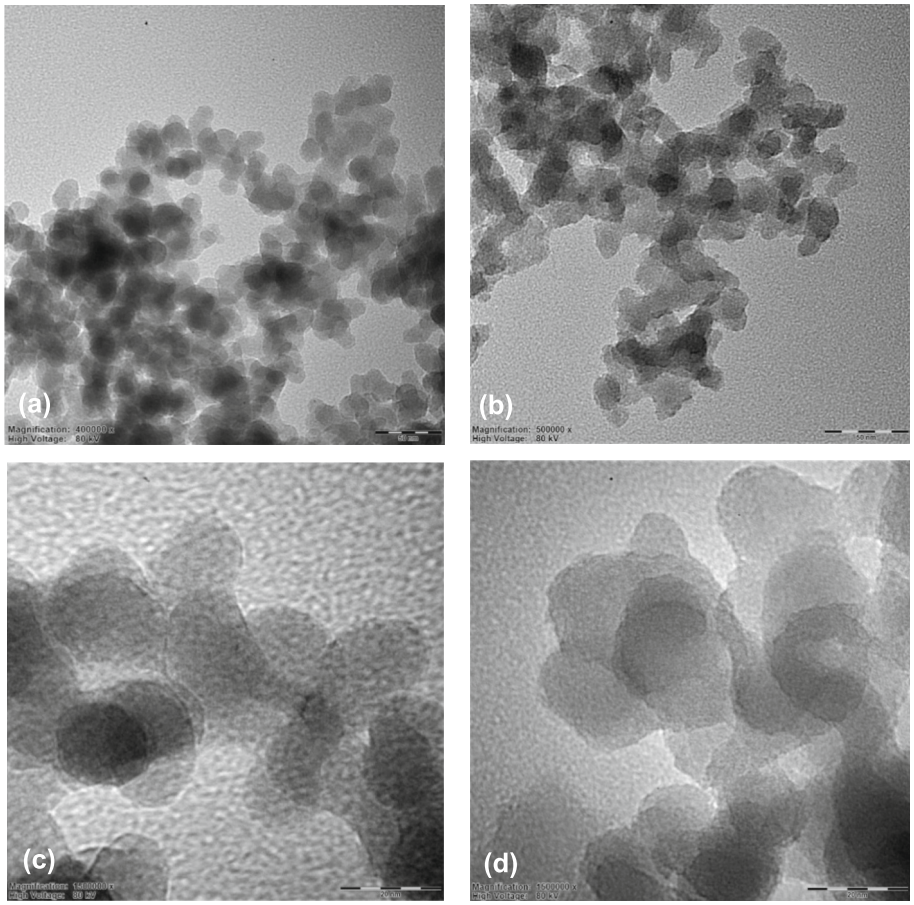


Fig. 5. TEM micrographs of silica nanoparticles: (a, c) bare silica nanoparticles exhibiting a smooth morphology with well-defined boundaries and (b, d) $NaBH_4$-treated surface-etched silica nanoparticles displaying roughened surfaces due to the etching process.

Table 1
Actual and projected surface area values of silica and etched silica nanoparticles obtained from AFM analysis.

Nanoparticle	Actual Surface Area	Projected Surface Area
Silica	4.142 μm^2	3.999 μm^2
Etched Silica	5.055 μm^2	3.999 μm^2

influenced the hydrodynamic size, consistent with TEM analysis. In contrast, bare silica nanoparticles show a higher mean size of 197.74 nm with a noticeable fraction of larger particles exceeding 400 nm. The reduction in mean size after etching confirms partial surface removal by $NaBH_4$, resulting in a more refined nanoparticle population. It should be noted that the average sizes obtained from DLS (>150 nm), and TEM (<50 nm) are not directly comparable due to the fundamental differences between the two techniques. TEM provides direct visualization of the primary nanoparticles under dry conditions, whereas DLS measures the hydrodynamic diameter of particles dispersed in solution. The latter reflects not only the particle core size but also the surrounding solvation layer and, more importantly, the presence of particle clusters. In this study, TEM images (Fig. 5) confirm that the nanoparticles are <50 nm in diameter, while the DLS data (Fig. 7a) indicate larger sizes because the particles form grape-like aggregates typical of precipitated silica (Fig. 4). This explains the apparent discrepancy and is consistent with the well-documented observation that DLS generally yields larger size values than TEM for colloidal silica nanoparticles [36].

The zeta potential analysis in Fig. 7b supports the DLS findings on particle surface characteristics. Etched silica nanoparticles (orange) exhibit a more negative peak at −52.01 mV, whereas bare silica nanoparticles (blue) peak at −43.97 mV. This indicates that bare silica has a lower surface charge density, while etched silica possesses a stronger negative charge due to surface chemistry modifications. The higher zeta potential of the etched silica, measured at pH 8.45 after dispersion (compared to pH 7.31 for the bare sample), reflects surface chemistry modifications. This elevated pH likely results from enhanced deprotonation of surface silanol groups ($Si–OH \rightarrow Si–O^- + H^+$) [37] and the introduction of additional negatively charged species during etching. While a higher (more negative) charge enhances colloidal stability by strengthening electrostatic repulsion between particles, it may also hinder dense particle accumulation at the oil–water interface. Nevertheless, two additional factors counterbalance this effect. FT-IR analysis confirmed the presence of hydrophobic functional groups on the etched silica surface, which are expected to facilitate migration toward the oil–water interface. In addition, etched nanoparticles exhibited smaller particle sizes, enabling more efficient interfacial seating compared to bare silica. These combined characteristics suggest that etched particles have the potential for superior interfacial performance, a hypothesis that is further examined in the subsequent emulsion stability analysis.

Overall, these morphological changes, consistent with DLS, XPS, and TEM analyses, confirm the structural transformation of the nanoparticles. The increased surface roughness and hydrophobicity enhance interfacial interactions (fluid-fluid or rock-fluid), improving their effectiveness in adsorption and catalysis.

3.2. Impact of nanoparticle modifications on emulsification

The impact of silica nanoparticle shape and surface roughness on

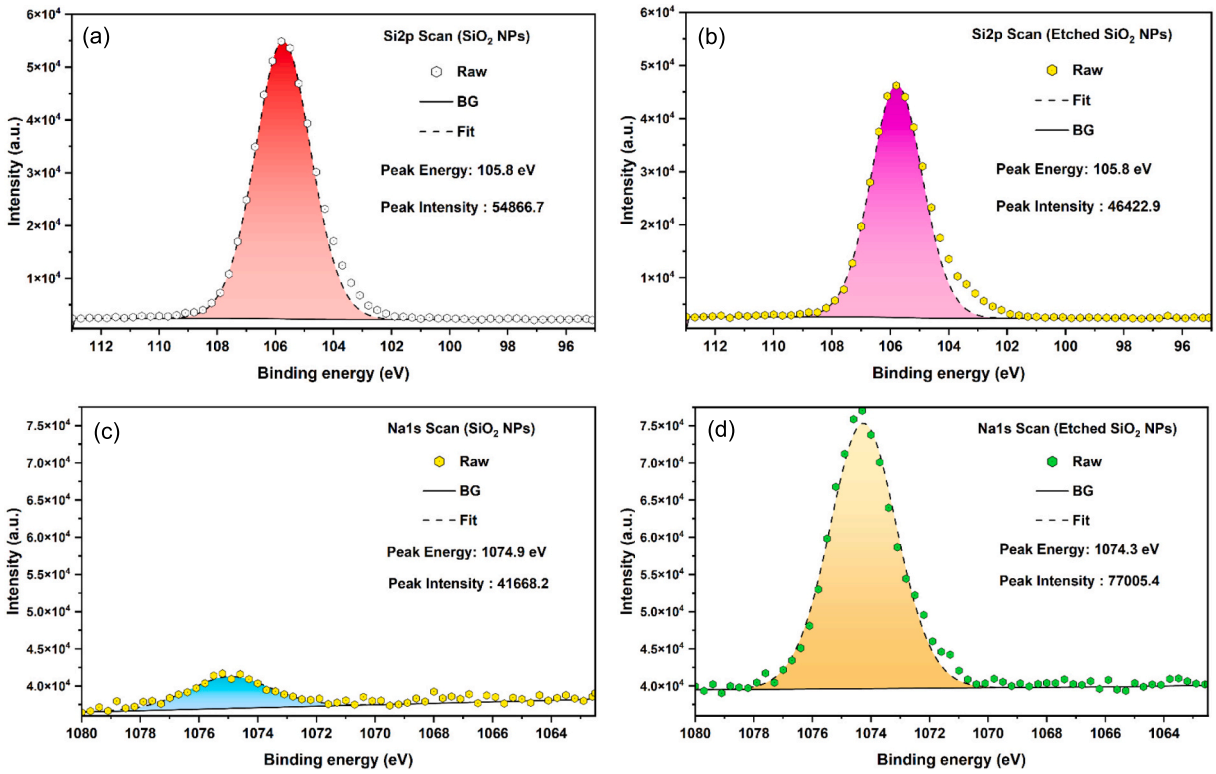


Fig. 6. XPS analysis of silica nanoparticles before and after etching: (a, b) Si2p scans showing decreased peak intensity after etching, confirming material loss; (c, d) Na1s scans revealing increased intensity after etching, indicating Na incorporation from $NaBH_4$ interaction (*BG: background*).

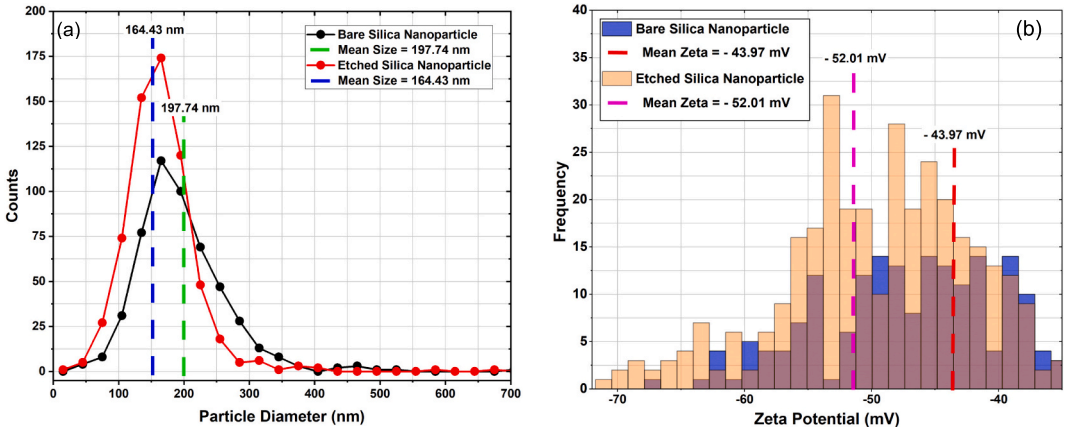


Fig. 7. (a) Particle size distribution of bare silica and etched silica, showing reduced size after etching. (b) Zeta potential distribution, indicating higher surface charge density for etched silica.

Pickering emulsion formation was explored, with a focus on surface etching effects on oil-water interface dynamics. Pickering emulsions are typically stabilized by solid particles at the oil-water interface, forming a mechanical barrier that prevents droplet coalescence [38]. We compared the effectiveness of 500 ppm nanofluids containing bare and surface-etched silica nanoparticles in stabilizing oil-in-water emulsions. Drop-by-drop addition of the oil phase while stirring at a low RPM (300 rpm) resulted in two distinct behaviors for the silica nanoparticles. Etched silica nanoparticles adhered to the oil droplets, leading to the formation of Winsor Type II emulsions [39]. Upon stopping stirring, this behaviour was characterized by oil accumulating at the top, emulsions forming in the middle, and a brownish nanofluid settling at the bottom (Fig. 8a). In contrast, for bare silica nanoparticles, no emulsion was formed. A plain oil phase remained at the top, and the nanofluid below was clear and colourless (Fig. 8b). When the systems were stirred at a higher RPM (2000 rpm) for two hours, both transitioned to Winsor Type I emulsions. This configuration was characterized by emulsions at the top, a brownish nanofluid in the middle, and a cleaner fluid at the bottom, though the separation was not as evident. Winsor Type I emulsions typically occur when oil is dispersed within water as the continuous phase [40]. The brownish middle layer suggested the presence of nanofluids and dispersed oil droplets in the water phase, while the cleaner bottom layer likely consisted of excess water with fewer particles or emulsions.

Figs. 8e (bare silica) and **8f** (etched silica) provide 1600× magnification microscopic evidence of nanoparticle adsorption at the oil-water interface. The rough texture surrounding the droplets in both images is a defining characteristic of Pickering emulsions, where solid particles

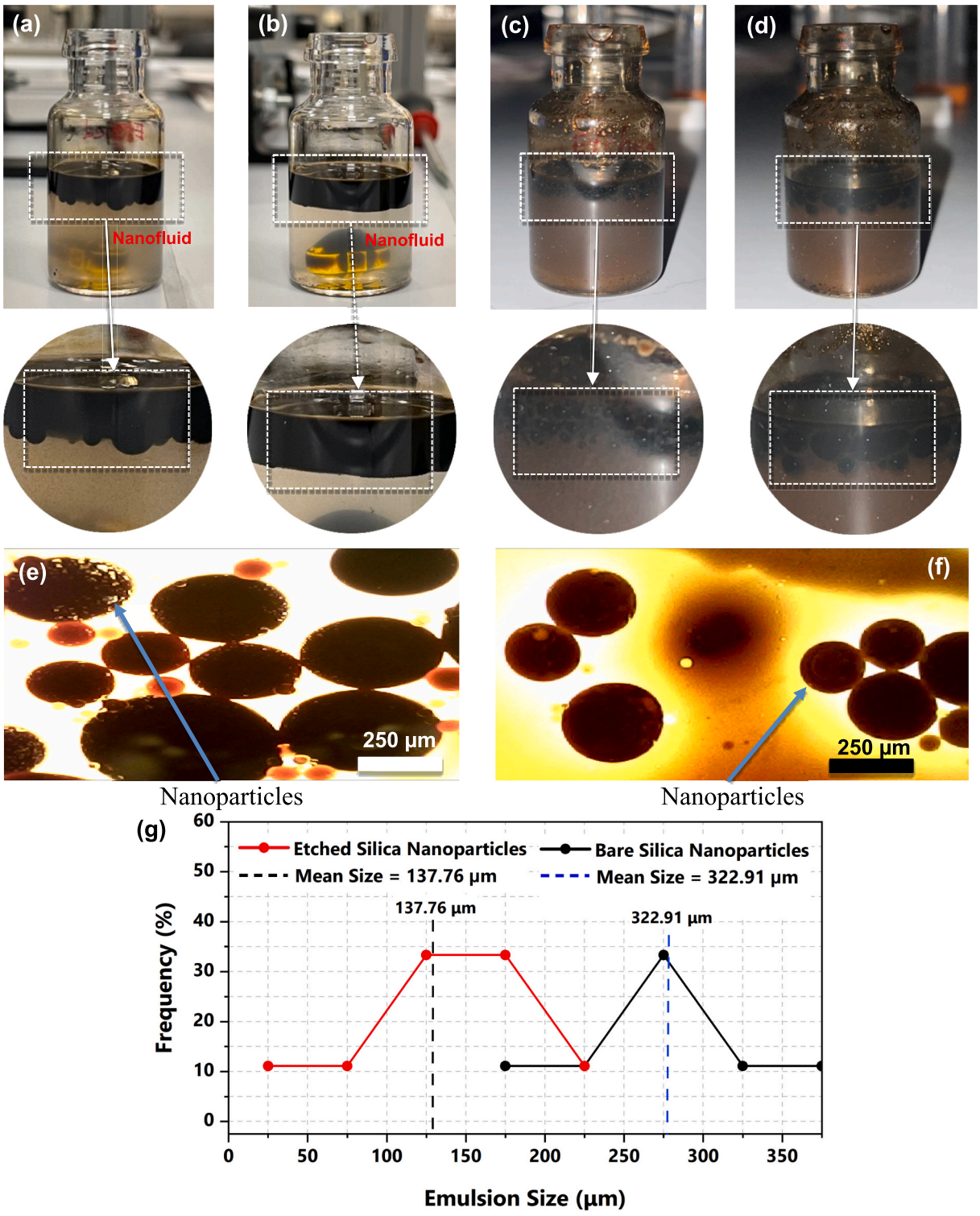


Fig. 8. (a) Winsor Type II emulsions with 500 ppm etched silica after low RPM stirring. (b) Behaviour of 500 ppm bare silica nanoparticles after low RPM stirring. (c) Winsor Type I emulsions with 500 ppm etched silica after high RPM stirring, showing smaller oil droplets. (d) Winsor Type I emulsions with 500 ppm bare silica after high RPM stirring, showing larger oil droplets. (e) Microscopic images of 500 ppm bare silica nanoparticles at the oil-water interface, showing a coarser texture and less uniform particle arrangement. (f) Microscopic images of 500 ppm etched silica nanoparticles adsorbed at the oil-water interface, highlighting their rough texture and uniform interfacial distribution. (g) Oil droplet size distribution for emulsions stabilized with 500 ppm etched and bare silica nanoparticles, showing smaller droplets with etched silica compared to larger ones with bare silica.

stabilize the interface and prevent coalescence, consistent with previous findings [41] [42]. Despite this shared feature, the emulsions differ in size and uniformity due to variations in nanoparticle adsorption and size, which influence nanoparticle mobility in the continuous phase and the curvature of Pickering emulsions. Complementing these observations, Fig. 8g presents the droplet size distribution, revealing that emulsions stabilized with etched silica nanoparticles form smaller droplets compared to the much larger droplets produced with bare

silica.

Larger nanoparticles exhibit higher bending resistance, making it more difficult for them to conform to the curvature of smaller oil droplets [43], thereby favouring the formation of larger emulsions. This relationship is described by Eq. (2) [44]:

$$k_r = 0.5 \times \sigma \times r_p^2 \left(0.68 \times \sin^4\theta + 5 \times \cos^2\theta - 0.875\right) \quad (2)$$

where k_r represents particle bending resistance, σ is the interfacial tension, r_p is the particle radius, and θ is the contact angle. The presence of r_p^2 in the equation indicates that bending resistance increases quadratically with particle size, meaning larger nanoparticles experience significantly greater resistance to conforming around small oil droplets [45]. Consequently, they are less effective at stabilizing emulsions with fine droplet sizes. Given that etched silica nanoparticles (mean size: 164.43 nm) are notably smaller than their bare silica counterparts (197.74 nm), their lower bending resistance enhances their ability to accommodate high interfacial curvature, resulting in finer oil-in-water Pickering emulsions. Another key factor might be nanoparticles' ability to rapidly diffuse to the interface. The diffusion coefficient of nanoparticles (D_{NPs}) is inversely proportional to the nanoparticle radius according to Einstein's formula [46]:

$$D_{NPs} = \frac{k_B \times T}{6\pi \times \mu \times r_p} \quad (3)$$

where D_{NPs} is the nanoparticle diffusion coefficient, k_B is the Boltzmann constant, T is absolute temperature, μ is nanofluid viscosity, and r is nanoparticle radius. As summarized in Table 2, the calculated diffusion coefficients indicate that smaller nanoparticles exhibit higher diffusion rates, enabling them to reach and adsorb onto the oil-water interface more rapidly. This accelerated adsorption, coupled with their lower bending resistance, enhances their ability to stabilize finer emulsions.

Fig. 9 presents the microscopic analysis of emulsions stabilized by bare (left) and surface-etched (right) silica nanoparticles at concentrations of 1000, 1500, 2000, and 2500 ppm.

The third column quantifies droplet size distribution and mean size, showing a shift toward smaller mean sizes and tighter distributions, particularly with etched silica. Across all concentrations, etched nanoparticles produce significantly smaller and more uniform droplets than bare silica, with a sharper reduction in mean droplet size and a narrower size distribution. Increasing nanoparticle concentration enhances stability for both types, but the effect is more pronounced with etched silica, which forms stronger interfacial layers that better prevent coalescence. Unlike surfactant-based emulsions, where excess surfactants beyond the critical micelle concentration (CMC) may lose effectiveness [47], nanoparticles stabilize emulsions through a different interfacial mechanism. Initially, nanoparticles adsorb onto the droplet surface, forming a rigid interfacial layer that prevents coalescence [48]. At higher concentrations, excess nanoparticles reinforce this barrier and further increase emulsion viscosity, aligning with the findings of Feng et al. [49]. Juarez and Whitby [50] similarly observed that emulsions were unstable at low particle concentrations due to partial interfacial coverage by silica nanoparticles. However, increasing the nanoparticle concentration led to well-separated and stable emulsions. It should be noted that the apparent differences in oil content across images at different nanoparticle concentrations are solely due to sample handling for microscopic observation. The emulsions were collected manually and placed on microscope slides for droplet size analysis; as droplets migrated or spread across the glass slide, the captured images did not always represent identical volumes of emulsions. This does not reflect a change in the oil-to-water ratio, which remained constant (2:3) throughout all experiments.

Table 2
Physicochemical properties of silica and etched silica nanoparticles, including the parameters used to calculate their diffusion coefficients (D_{NPs}) using Einstein's formula.

Nanoparticle	k_B (J/K)	Temperature (K)	Viscosity (Pa.s)	r_p (m)	D_{NPs} (m^2/s)
Silica	1.38×10^{-23}	298.15	1×10^{-3}	98.87×10^{-9}	2.21×10^{-12}
Etched Silica	1.38×10^{-23}	298.15	1×10^{-3}	82.15×10^{-9}	2.65×10^{-12}

The superior emulsification efficiency of surface-etched silica nanoparticles stems from their increased surface roughness (AFM) and altered morphology (SEM/TEM). These structural changes, along with reduced hydrophilicity (FT-IR/XPS), enhance mechanical anchoring at the oil-water interface, improving droplet stabilization and yielding finer emulsions. This phenomenon can be explained by a formula proposed by Binks and Lumsdon [45]:

$$r_e = \frac{4 \times r_p \times V_w}{V_p} \quad (4)$$

where the emulsion droplet radius (r_e) is inversely proportional to the nanoparticle volume fraction (V_p) and directly proportional to the nanoparticle radius (r_p). As the nanoparticle concentration increases from 1000 ppm to 2500 ppm, V_p of nanoparticles rises, leading to a reduction in the emulsion droplet radius (r_e) for a given water volume (V_w), as described by Eq. (4). While this trend holds for both bare and surface-etched silica nanoparticles, the latter exhibit superior emulsification performance due to their smaller particle size (164.43 nm). Their finer dimensions enable greater surface coverage at the oil-water interface, forming a denser and more robust barrier against droplet coalescence. This enhanced stabilization results in smaller and more uniform droplets, further supporting the role of tailored surface modifications in optimizing nanoparticle-based emulsion stabilizers. These findings collectively highlight the efficiency of surface-etched silica nanoparticles in emulsification, driven by their increased surface roughness and reduced hydrophilicity, as confirmed by previous AFM, FT-IR, and XPS analyses.

3.3. Emulsion stability comparison of bare and etched nanoparticles

Emulsion stability of 1000 ppm bare silica and surface-etched silica nanoparticles was monitored over time, and the results are shown in Fig. 10. The left column represents emulsions stabilized by bare silica nanoparticles, while the right column corresponds to emulsions stabilized by surface-etched silica nanoparticles. The images were taken immediately after emulsification, after 1 h, and after 2 h to observe changes in droplet size distribution and stability. Initially, the surface-etched silica-stabilized emulsion (right column) exhibits a more uniform droplet size distribution, with smaller, well-dispersed droplets. After 1 h, the droplets remain relatively stable, with only minor coalescence observed. Even after 2 h, the emulsion maintains its structural integrity, with minimal increase in droplet size, indicating better stabilization. In contrast, the bare silica-stabilized emulsion (left column) shows a more polydisperse droplet distribution right after emulsification, with noticeable variation in droplet sizes. After 1 h, droplet coalescence begins, leading to the formation of larger clusters. By 2 h, significant droplet aggregation and merging occur, forming irregular structures with a much broader droplet size distribution. This destabilization behaviour aligns with prior reports: Gholinezhad et al. [14] observed that at 1000 ppm bare SiO_2 nanoparticles, roughly 81.5 % of an n-octane emulsion disappeared within 1–2 h, mirroring our results.

The altered shape of the nanoparticles may be a key factor contributing to the enhanced stability observed in the surface-etched silica-stabilized emulsions. The deviation from a perfectly spherical geometry to a rough, non-spherical surface likely facilitates tighter attachment at the oil–water interface. The etched particles may interlock through their surface dents—much like gears—forming a mechanically interlocked

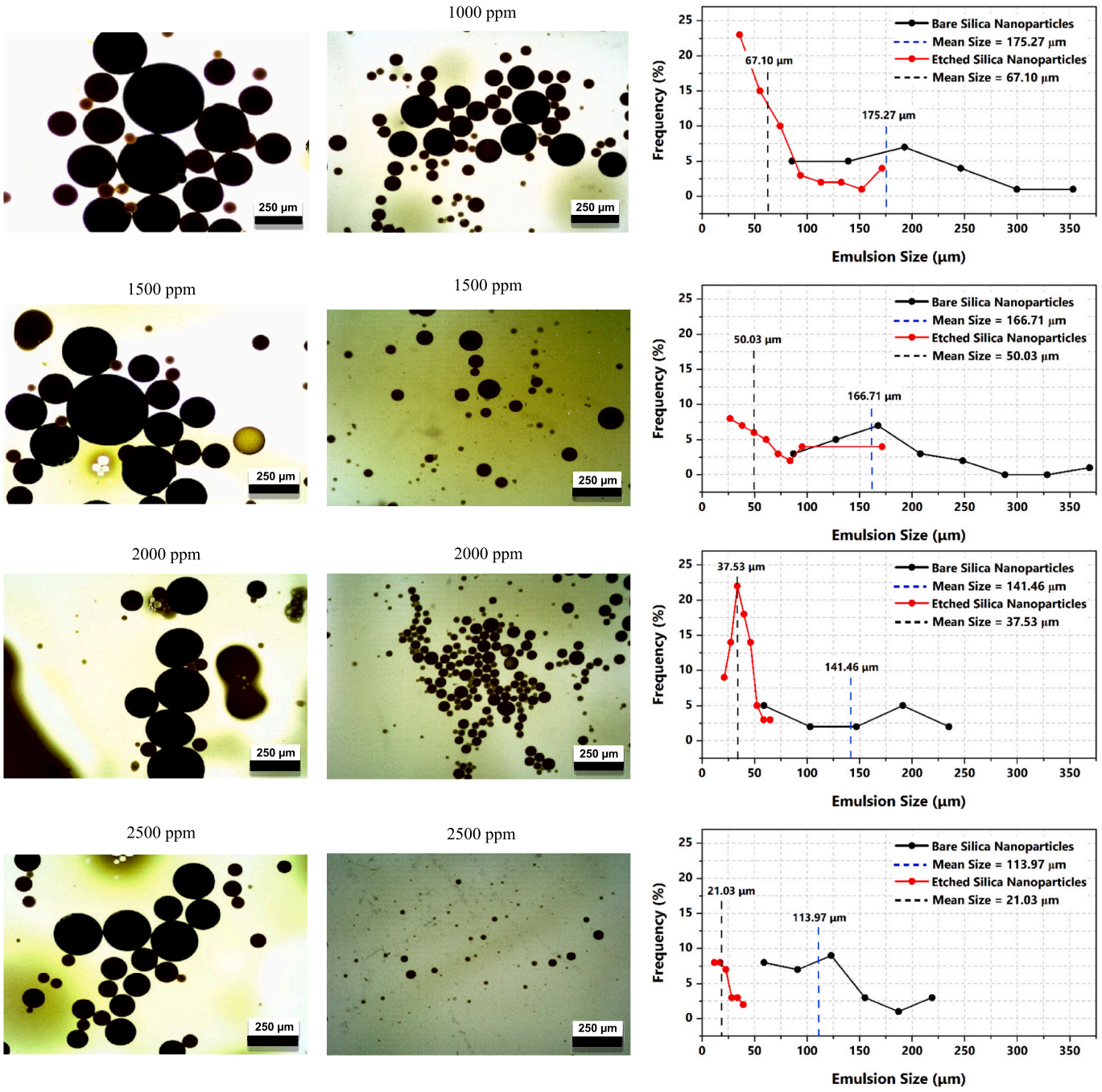


Fig. 9. Optical micrographs (left and middle columns) and corresponding size distribution plots (right column) illustrating the effect of nanoparticle concentration on emulsion stability for bare silica nanoparticles (left) and etched silica nanoparticles (middle) at different concentrations (1000 ppm, 1500 ppm, 2000 ppm, and 2500 ppm).

interfacial layer that resists coalescence more effectively than smooth, spherical particles. This interpretation is consistent with the findings of Madivala et al. [51], who investigated the role of particle shape in emulsion stabilization. Their study demonstrated that elliptical polystyrene particles outperformed spherical counterparts in stabilizing Pickering emulsions. Similarly, Kalashnikova et al. [52] reported that cellulose nanorods were highly effective in forming super-stable Pickering emulsions by assembling into bridge-like structures at the interface. These observations support the hypothesis that the enhanced interfacial behaviour of etched silica nanoparticles arises from their shape and surface morphology.

In contrast, the progressive coalescence observed in the bare silica-stabilized system suggests weaker interfacial stabilization. Dynamic interfacial tension measurements show that over 20 min (Fig. 11), the oil–water IFT with bare silica nanoparticles decreased only slightly, from 38 ± 1 to 35 ± 1 mN/m (~7.9 % reduction), whereas the modified nanoparticles produced a more pronounced drop to 26 ± 1 mN/m (~31.6 % reduction). This corresponds to nearly four times greater IFT reduction, confirming the stronger interfacial activity of the modified nanoparticles. Comparable results have been reported in the literature. Hosseini et al. [53] observed that bare silica nanoparticles led to only a relatively low reduction in IFT, insufficient to strongly influence oil recovery efficiency. In contrast, Golshokooh et al. [54] found no change in IFT between crude oil and fumed silica nanofluids even at high

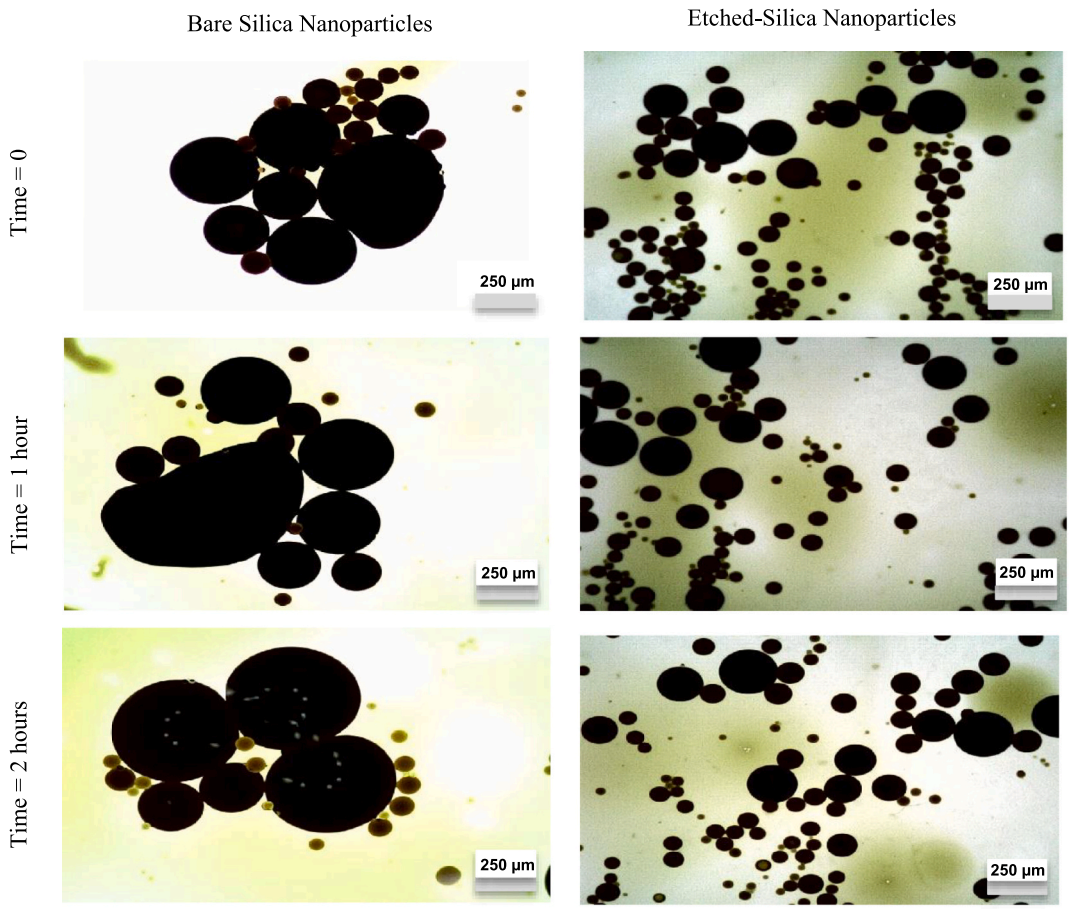


Fig. 10. Optical micrographs showing the stability of emulsions stabilized by 1000 ppm bare silica nanoparticles (left column) and surface-etched silica nanoparticles (right column) over time. Images were captured immediately after emulsification (top row), after 1 h (middle row), and after 2 h (bottom row).

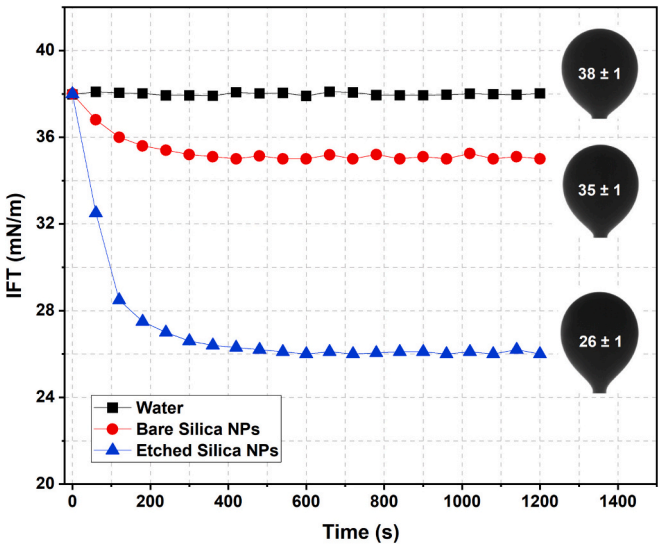


Fig. 11. Dynamic oil–nanofluid interfacial tension measurements, demonstrating the enhanced interfacial activity of etched silica nanoparticles (NPs) compared to bare silica NPs.

concentrations up to 200,000 ppm, highlighting the limited ability of unmodified silica to alter oil–water interfacial properties. This weak performance can be attributed to the strong hydrophilicity of bare silica, which prevents stable adsorption at the oil–water interface and thus minimizes its capacity to reduce IFT. By contrast, surface-modified silica nanoparticles bearing hydrophobic functional groups demonstrate markedly greater activity at the oil–water interface. Hydrophobization enhances partial wettability balance, lowering the energy barrier for adsorption and promoting stronger anchoring of nanoparticles at the interface. Wang et al. [55] recently demonstrated that grafting thiol and dodecyl functional groups onto silica surfaces leads to substantial reductions in IFT, thereby enhancing Pickering emulsion stability and interfacial reinforcement. Similarly, Xu et al. [56] reported that silica nanoparticles functionalized with alkyl chains of varying lengths significantly reduced the IFT at the n-octane/water interface, with an optimum effect observed at a concentration of 1000 ppm. These findings are consistent with the enhanced performance of the modified nanoparticles in the present study.

This different IFT reduction behaviour can be ascribed to the lower desorption energy of bare nanoparticles from the oil–water interface, which is defined as [57]:

$$E_D = \pi \times r_p^2 \times \sigma_{ow} \times (1 - \cos\theta)^2 \quad (5)$$

where θ is the contact angle, r_p is the particle radius, and σ_{ow} is the oil-water interfacial tension. Anchoring energy (E_D) reaches its maximum at $\theta = 90^\circ$ and declines sharply as θ deviates from this point. For instance, E_D falls below 10 kT when θ exceeds 150° or drops below 15° (see Fig. 12a). This suggests that amphiphilic or partially hydrophobic nanoparticles are more effective in maximizing nanoparticle anchoring strength, whereas hydrophilic nanoparticles fail to exhibit sufficient interfacial activity. Consistent with this, Briggs et al. [58] reported the formation of exceptionally small oil-in-water Pickering emulsions using multi-walled carbon nanotubes with moderate hydrophobicity. The

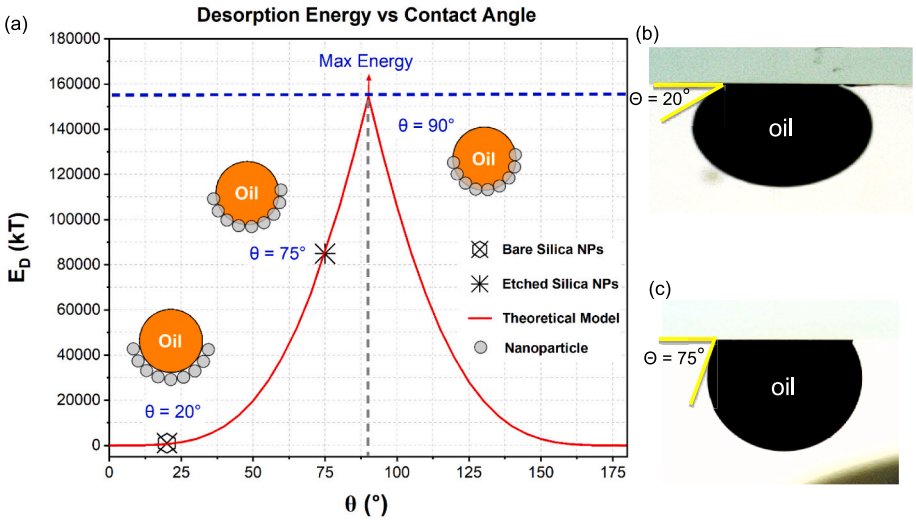


Fig. 12. (a) Desorption energy (E_D) as a function of contact angle (θ) for silica nanoparticles at the oil-water interface. Theoretical predictions (red curve) align closely with calculated values, showing maximum anchoring energy at $\theta = 90°$ and significant reductions under highly hydrophilic ($\theta = 20°$) or weakly water-wet (θ = 75°) conditions. (b) Optical image showing the contact angle ($\theta = 20°$) of bare silica nanoparticles, confirming a strongly water-wet surface. (c) Contact angle measurement ($\theta = 75°$) for etched silica nanoparticles, indicating a weakly water-wet condition. (For interpretation of the references to colour in this figure legend, the reader is referred to the web version of this article.)

enhanced performance was attributed to their stronger adsorption at the interface, which effectively prevented droplet coalescence and contributed to the reduction in droplet size. Therefore, we hypothesize that surface-modified silica nanoparticles, with enhanced hydrophobicity and increased surface roughness, are better suited for improving interfacial interactions. To validate this hypothesis, a thin film of both silica and etched silica nanoparticles was coated on two glass slides. The slides were dried under ambient conditions, and the three-phase contact angle at the glass (solid)–water (bulk)–crude oil (drop) interface was then measured. As shown in Fig. 12b, bare silica nanoparticles exhibited a strongly water-wet condition with $\theta = 20 \pm 1°$, whereas etched silica nanoparticles displayed a weakly water-wet condition with $\theta = 75 \pm 1°$ (Fig. 12c). This confirms the enhanced interfacial activity of etched silica nanoparticles, attributed to increased hydrophobicity from PVP's carbon functional groups, which improve droplet stabilization by modifying nanoparticle wettability. Conversely, bare silica nanoparticles, being highly hydrophilic, struggle to anchor in an oil-rich environment, leading to faster droplet coalescence and reduced stability.

Another factor could be the variation in surface roughness between bare and etched nanoparticles, which influences interfacial adsorption and affects their ability to anchor at the oil-water interface. According to Wenzel's equation ($\cos\theta_{rough} = r_f \times \cos\theta_{smooth}$) [59], surface roughness (r_f) modifies the apparent contact angle (θ_{rough}) relative to the intrinsic Young's contact angle (θ_{smooth}). The roughness factors (r_f) obtained from AFM analysis were 1.035 for bare silica and 1.264 for etched silica, leading to intrinsic contact angles of 24.87 ± 1° and 78.18 ± 1°, respectively. This indicates that surface roughness slightly reduced the hydrophobicity of both nanoparticles and made the systems more water-wet. Since 90° is the optimal condition for anchoring (Fig. 12a), this observation suggests that rougher surfaces may have opposing effects depending on the initial wettability of the material. Thus, it can be argued that surface roughness plays a dual role in nanoparticle adsorption: it can enhance interfacial anchoring when the initial contact angle is sufficiently high but may hinder attachment when the surface is already hydrophilic. Understanding this balance is crucial for optimizing nanoparticle performance in stabilizing emulsions or modifying interfacial properties.

Incorporating all relevant parameters into Eq. 5, the final desorption energy values were determined to be ~ 3.91×10^{-18} J for bare silica and ~ 3.49×10^{-16} J for etched silica (Fig. 12a), with interfacial tensions of 35 ± 1 and 26 ± 1 mN/m, respectively. Notably, the desorption energy for etched silica is two orders of magnitude higher than that of bare silica, indicating significantly stronger nanoparticle adhesion at the oil-water interface. This substantial increase confirms the enhanced interfacial stability of etched silica and theoretically validates the success of surface etching in improving nanoparticle performance for interfacial applications. Furthermore, the calculated desorption energy values closely match the theoretical model (red curve) in Fig. 12a, demonstrating a consistent trend where nanoparticle adhesion strength peaks around 90° contact angle and declines for more hydrophilic conditions (θ = 20°). This agreement reinforces the role of surface roughness, wettability, and interfacial tension in governing nanoparticle adhesion at the oil-water interface.

3.3.1. *Pore-scale oil recovery results*

Microfluidic experiments were conducted using a glass micromodel fully saturated with crude oil (Fig. 13a), visually represented as a dark-coloured network, to assess the impact of the developed silica nanofluid on oil recovery at both macroscopic and pore scales. Fig. 13b shows oil displacement with bare silica nanoparticles, where the injected fluid mobilizes the oil but leaves significant residual saturation due to weaker interfacial interactions. These highly hydrophilic nanoparticles are ineffective at disrupting oil films, resulting in lower oil recovery compared to surfactants. In contrast, flooding with etched silica nanoparticles (Fig. 13c) leads to more efficient oil displacement, driven by reduced hydrophilicity and increased surface roughness, which may aid in mechanical oil sweeping. This behaviour is similar to that of graphene oxide nanosheets, where sharp edges facilitate oil detachment [60]. In contrast, the smooth, spherical shape of bare silica nanoparticles leads to lower interfacial friction, reducing their ability to mobilize oil [2]. The increased roughness of etched silica nanoparticles enhances their ability to disrupt oil films and mobilize trapped oil. The enhanced oil removal is reflected in the increased presence of pure green regions in Fig. 13c, indicating greater oil recovery, whereas Fig. 13b shows more dark-green areas, highlighting higher residual oil retention.

The pore-scale behaviour of etched silica and silica nanofluid was also examined to reveal distinct wettability and emulsion formation characteristics that influence microscopic and macroscopic oil recovery performance. Figs. 13d–f show that etched silica promotes stable oil-in-

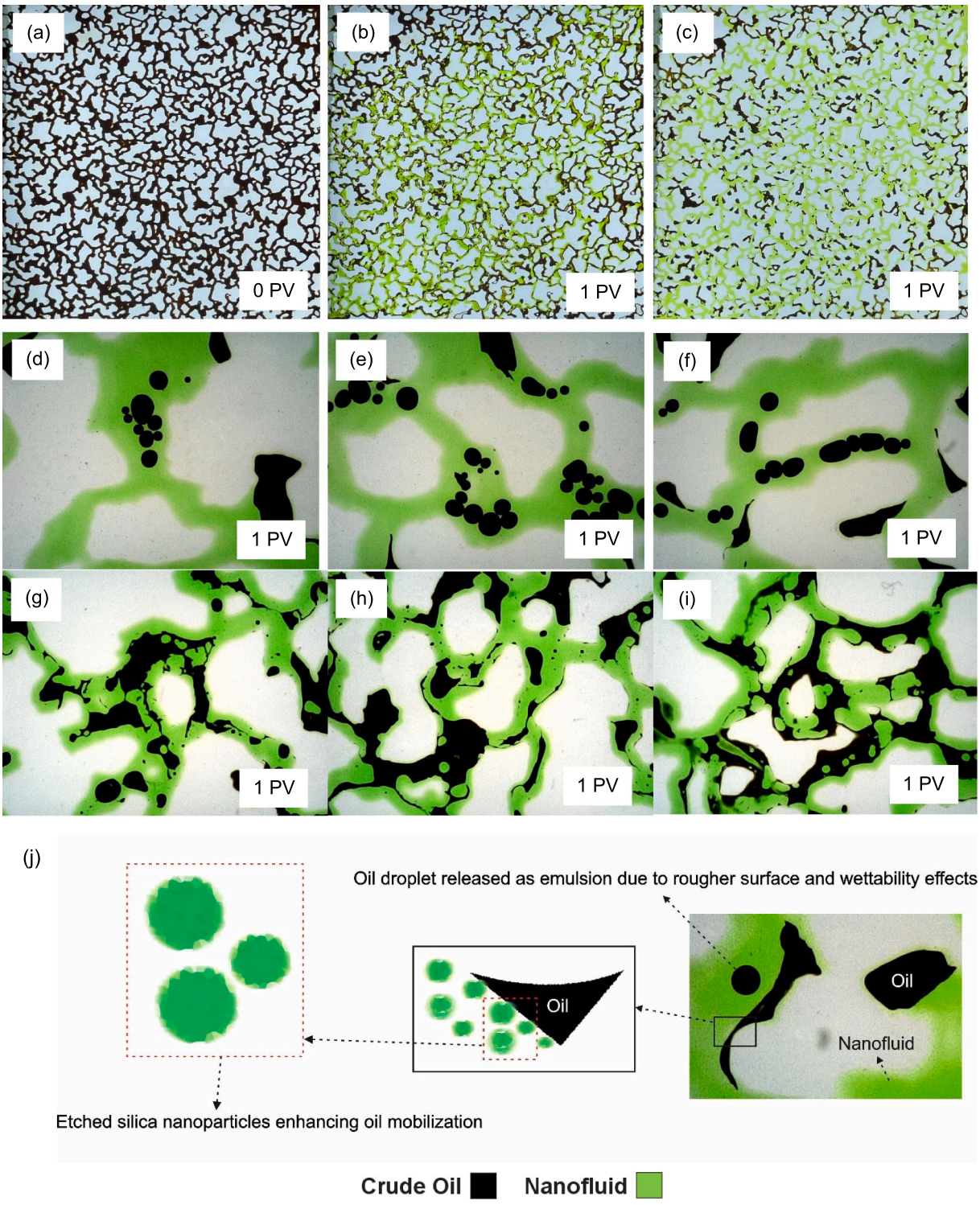


Fig. 13. (a) Glass micromodel fully saturated with crude oil. (b) Oil displacement using bare silica nanoparticles, showing residual oil trapping. (c) Etched silica flooding, enhancing wettability contrast and oil recovery. (d–f) Etched silica promoting oil-in-water emulsions, reducing residual trapping. (g–i) Silica nanofluid inducing water-in-oil emulsions, altering flow pathways and affecting oil displacement. (j) Schematic representation of etched silica nanoparticles enhancing oil mobilization through roughness-induced emulsification, illustrating the release of oil droplets into the aqueous phase.

water emulsions, consistent with bulk emulsion experiments, indicating increased oil-wet behaviour that reduces oil adhesion to the rock surface. Moderately oil-wet nanoparticles break the oil phase into smaller droplets and reduce residual trapping, thereby enhancing oil recovery. Conversely, Figs. 13g–i illustrate how the inherently water-wet silica nanofluid promotes water-in-oil emulsions, resulting in water phase fragmentation and entrapment within the continuous oil phase. This restriction of water mobility alters flow pathways, preserving oil continuity in the pore network and leading to a decrease in overall displacement efficiency.

Beyond enhanced mechanical interactions, the contrasting behaviors observed in the micromodel experiments can be attributed to the smaller

size and more negative charge of the etched silica nanoparticles. This superior performance can be further explained by the concept of structural disjoining pressure. According to classic theory, the disjoining pressure (Π_d) of a thin liquid film on a flat surface is given by [61]:

$$\Pi_d = -\frac{A_H}{6\pi \times h^3} \quad (6)$$

where A_H is the Hamaker constant (J), and h is the liquid film thickness (m). For silica, A_H was taken as 7×10^{-23} J [62], and h for each nanoparticle type was assumed to be their average diameter, representing a single layer of nanoparticles positioned at the nanofluid-solid interface. Using this model, the disjoining pressure was calculated for untreated and etched silica nanoparticles as approximately -4.81×10^{-4} Pa and -8.38×10^{-4} Pa, respectively. The increased negative disjoining pressure for etched silica nanoparticles indicates stronger attractive forces at the oil-water-glass interface, promoting oil detachment and enhancing in-situ oil-in-water emulsion formation (Fig. 13j). These findings align with the experimental results, where etched silica nanoparticles exhibited superior oil recovery due to their ability to destabilize oil films and modify wettability conditions, thereby improving oil displacement efficiency.

4. Conclusions

This study introduces a novel method using $NaBH_4$ to modify silica nanoparticles, enhancing their surface properties for improved oil displacement and emulsification. The results show that etched silica nanoparticles facilitate Winsor Type II emulsions at low stirring rates, while bare silica is ineffective. At higher stirring rates, both systems form Winsor Type I emulsions, but etched nanoparticles produce smaller, more stable droplets, indicating superior emulsification performance. This enhancement is attributed to the nanoparticles' smaller size, lower bending resistance, and higher diffusion rates, which enable better accommodation at the oil-water interface. The altered shape and increased surface roughness of the etched silica particles contribute to stronger interfacial attachment, as they interlock more effectively at the interface, confirmed by desorption energy values of $\sim 3.49 \times 10^{-16}$ J for etched silica versus $\sim 3.91 \times 10^{-18}$ J for bare silica.

In pore-scale microfluidic oil recovery, surface-etched silica nanoparticles outperform bare silica due to their smaller size, greater negative charge, and superior mechanical interactions at the oil-water interface. The higher structural disjoining pressure of -8.38×10^{-4} Pa for etched silica, compared to -4.81×10^{-4} Pa for bare silica, improves oil phase stabilization, leading to better mobilization, reduced residual oil saturation, and higher oil recovery. These findings highlight that this chemical-based approach, unexplored in oil recovery, offers a new pathway for enhanced oil mobilization and emulsion stability. It can also be extended to nanoparticle-based applications in catalysis, wastewater treatment, CO_2 sequestration [63] [64] [65], pharmaceuticals, and other industries.

Looking ahead, further validation under core-scale conditions is necessary to translate these findings into field-relevant insights. Future work will therefore focus on core flooding experiments to evaluate pressure response, water cut, and oil recovery efficiency, thereby bridging the gap between microfluidic observations and reservoir-scale applications. Such efforts will provide a more comprehensive assessment of the practical EOR potential of these modified nanoparticles.

CRediT authorship contribution statement

Reza Khoramian: Writing – original draft, Methodology, Formal analysis, Data curation. **Kamila Ganiyeva:** Methodology, Formal analysis, Data curation. **Miras Issakhov:** Investigation, Formal analysis, Data curation. **Peyman Pourafshary:** Writing – review & editing, Validation, Supervision, Investigation, Formal analysis. **Saule Aidarova:** Writing – review & editing, Supervision, Resources. **Altynay Sharipova:** Writing – review & editing, Validation, Supervision, Resources.

Declaration of competing interest

The authors declare that they have no known competing financial interests or personal relationships that could have appeared to influence the work reported in this paper.

Acknowledgements

We sincerely thank the Science Committee of the Ministry of Science and Higher Education of the Republic of Kazakhstan for funding this research under grant IRN BR21882301. We also extend our gratitude to Mr. Gani Aktanov, Semey, Kazakhstan, for his assistance in cutting and drilling glass plates for micromodels and to Laser Kazemi, Pamenar, Tehran, Iran, for etching the patterns.

Data availability

No external data were used in the preparation of this research. All relevant information and findings are fully included within the manuscript.

References

[1] A.A. Isari, A. Ghaffarkhah, S.A. Hashemi, H. Yousefian, O.J. Rojas, M. Arjmand, A journey from structured emulsion templates to multifunctional aerogels, Adv. Funct. Mater. 34 (44) (2024) 2402365.
[2] R. Khoramian, R. Kharrat, S. Golshokooh, The development of novel nanofluid for enhanced oil recovery application, Fuel 311 (2022) 122558.
[3] Y. Hu, Y. Cao, F.M. Nguyen, B.D. Frank, M.J. Kalinowski, M. Li, S. Rajani, B. Marelli, Antibody-targeted phytohormone delivery using foliar sprayed silk fibroin Pickering emulsions, Adv. Funct. Mater. 34 (38) (2024) 2402618.
[4] M. Xiao, A. Xu, T. Zhang, L. Hong, Tailoring the wettability of colloidal particles for Pickering emulsions via surface modification and roughness, Front. Chem. 6 (2018) 225.
[5] M. Deshmukh, A. Pathan, Advancements and challenges in the use of surfactants and nanoparticles for enhanced oil recovery: mechanisms, synergies, and field applications, Environ. Sci. Pollut. Res. (2025) 1–35.
[6] K. Glosz, A. Stolarczyk, T. Jarosz, Siloxanes—versatile materials for surface functionalisation and graft copolymers, Int. J. Mol. Sci. 21 (17) (2020) 6387.
[7] J. Lee, S.H. Jo, J. Lim, Effect of surface modification of $CaCO_3$ nanoparticles by a silane coupling agent methyltrimethoxysilane on the stability of foam and emulsion, J. Ind. Eng. Chem. 74 (2019) 63–70.
[8] S. Maaref, A. Kantzas, S.L. Bryant, The effect of silanization assisted nanoparticle hydrophobicity on emulsion stability through droplet size distribution analysis, Chem. Eng. Sci. 201 (2019) 175–190.
[9] R. Khoramian, M. Nurmyrza, W. Lee, Chemical enhanced oil recovery using carbonized ZIF-67 MOFs and sulfonated copolymers at high reservoir temperatures, Chem. Eng. J. 499 (2024) 156653.
[10] Y.I. Alkotzer, F. Grzegorzewski, E. Belausov, E. Zelinger, G. Mechrez, In situ interfacial surface modification of hydrophilic silica nanoparticles by two organosilanes leading to stable Pickering emulsions, RSC Adv. 9 (68) (2019) 39611–39621.
[11] M.Z. Rong, M.Q. Zhang, H.B. Wang, H.M. Zeng, Surface modification of magnetic metal nanoparticles through irradiation graft polymerization, Appl. Surf. Sci. 200 (1–4) (2002) 76–93.
[12] C.A.J. Lin, R.A. Sperling, J.K. Li, T.Y. Yang, P.Y. Li, M. Zanella, W.H. Chang, W. J. Parak, Design of an amphiphilic polymer for nanoparticle coating and functionalization, Small 4 (3) (2008) 334–341.
[13] A. Kaiser, T. Liu, W. Richtering, A.M. Schmidt, Magnetic capsules and Pickering emulsions stabilized by core− shell particles, Langmuir 25 (13) (2009) 7335–7341.
[14] S. Gholinezhad, A. Kantzas, S.L. Bryant, Effect of surface functionalized silica nanoparticles on interfacial behavior: wettability, interfacial tension and emulsification characteristics, J. Mol. Liq. 349 (2022) 118220.
[15] L. Qi, C. Song, T. Wang, Q. Li, G.J. Hirasaki, R. Verduzco, Polymer-coated nanoparticles for reversible emulsification and recovery of heavy oil, Langmuir 34 (22) (2018) 6522–6528.
[16] J. Müller, K.N. Bauer, D. Prozeller, J. Simon, V. Mailänder, F.R. Wurm, S. Winzen, K. Landfester, Coating nanoparticles with tunable surfactants facilitates control over the protein corona, Biomaterials 115 (2017) 1–8.
[17] Y. Zhu, J. Jiang, K. Liu, Z. Cui, B.P. Binks, Switchable Pickering emulsions stabilized by silica nanoparticles hydrophobized in situ with a conventional cationic surfactant, Langmuir 31 (11) (2015) 3301–3307.

[18] X.Q. Wei, W.J. Zhang, L. Lai, P. Mei, L.M. Wu, Y.Q. Wang, Different cationic surfactants-modified silica nanoparticles for Pickering emulsions, J. Mol. Liq. 291 (2019) 111341.
[19] W. Yu, L. Sisi, Y. Haiyan, L. Jie, Progress in the functional modification of graphene/graphene oxide: A review, RSC Adv. 10 (26) (2020) 15328–15345.
[20] J. Liu, S. Chen, Y. Liu, B. Zhao, Progress in preparation, characterization, surface functional modification of graphene oxide: A review, J. Saudi Chem. Soc. 26 (6) (2022) 101560.
[21] L. Nayak, M. Rahaman, R. Giri, Surface modification/functionalization of carbon materials by different techniques: an overview, Carbon-Containing Polymer Composites (2018) 65–98.
[22] R. Khoramian, S.A. Ramazani, A., Hekmatzadeh, M., Kharrat, R. and Asadian, E., Graphene oxide nanosheets for oil recovery, ACS Applied Nano Materials 2 (9) (2019) 5730–5742.
[23] J. Kim, L.J. Cote, F. Kim, W. Yuan, K.R. Shull, J. Huang, Graphene oxide sheets at interfaces, J. Am. Chem. Soc. 132 (23) (2010) 8180–8186.
[24] X. Chen, X. Song, J. Huang, C. Wu, D. Ma, M. Tian, H. Jiang, P. Huang, Phase behavior of Pickering emulsions stabilized by graphene oxide sheets and resins, Energy Fuel 31 (12) (2017) 13439–13447.
[25] Q. Zhang, I. Lee, J. Ge, F. Zaera, Y. Yin, Surface-protected etching of mesoporous oxide shells for the stabilization of metal Nanocatalysts, Adv. Funct. Mater. 20 (14) (2010) 2201–2214.
[26] X. Du, J. He, A self-templated etching route to surface-rough silica nanoparticles for superhydrophobic coatings, ACS Appl. Mater. Interfaces 3 (4) (2011) 1269–1276.
[27] S.H. Ahmadi, B. Ding, S.L. Bryant, A. Kantzas, Transport dynamics of magnetic Pickering nanoemulsions within porous media: an experimental investigation, Colloids Surf. A Physicochem. Eng. Asp. 709 (2025) 136188.
[28] R. Khoramian, P. Pourafshary, S. Golshokooh, R. Kharrat, Optimizing synthetic core plugs: sintered glass beads and sand particles for natural rock property replication in fluid flow and reservoir studies, Geoenergy Science and Engineering 235 (2024) 212727.
[29] S.I. Kim, W.J. Kim, J.G. Kang, D.W. Kim, Intermolecular interaction engineering to enhance lithium-ion storage in two-dimensional oxidized silicon nanosheet anodes, Chem. Eng. J. 467 (2023) 143364.
[30] Y. Zhang, H. Jiang, Q. Wang, C. Meng, In-situ hydrothermal growth of $Zn4Si_2O_7(OH)_2 \cdot H_2O$ anchored on 3D N, S-enriched carbon derived from plant biomass for flexible solid-state asymmetrical supercapacitors, Chem. Eng. J. 352 (2018) 519–529.
[31] Y. Huang, W. Zhang, M. Zhang, X. Zhang, Y. Zhao, Hydroxyl-functionalized TiO_2@ SiO_2@ Ni/nZVI nanocomposites fabrication, characterization and enhanced simultaneous visible light photocatalytic oxidation and adsorption of arsenite, Chem. Eng. J. 338 (2018) 369–382.
[32] Y. Wang, W. Ma, D. Wang, Q. Zhong, Study on the reaction mechanism of the propylene oxide rearrangement via in situ DRIFTS, Chem. Eng. J. 307 (2017) 1047–1054.
[33] S.M. Lam, K.C. Chew, J.C. Sin, H. Zeng, H. Lin, H. Li, J.W. Lim, A.R. Mohamed, Ameliorated photodegradation performance of polyethylene and polystyrene films incorporated with ZnO-PVP catalyst, J. Environ. Chem. Eng. 10 (3) (2022) 107594.
[34] T.J. Ko, S.J. Park, M.S. Kim, S.M. Yoon, S.J. Kim, K.H. Oh, S. Nahm, M.W. Moon, Single-step plasma-induced hierarchical structures for tunable water adhesion, Sci. Rep. 10 (1) (2020) 874.
[35] H. Zhang, Y. Zhou, Y. Li, T.J. Bandosz, D.L. Akins, Synthesis of hollow ellipsoidal silica nanostructures using a wet-chemical etching approach, J. Colloid Interface Sci. 375 (1) (2012) 106–111.
[36] J. Lim, S.P. Yeap, H.X. Che, S.C. Low, Characterization of magnetic nanoparticle by dynamic light scattering, Nanoscale Res. Lett. 8 (1) (2013) 381.
[37] P. Allongue, C.H. de Villeneuve, S. Morin, R. Boukherroub, D.D. Wayner, The preparation of flat H–Si (111) surfaces in 40% NH4F revisited, Electrochim. Acta 45 (28) (2000) 4591–4598.
[38] Y. Qu, D. Sun, Y. Yu, Interfacial engineering in Pickering emulsion photocatalytic microreactors: from mechanisms to prospects, Chem. Eng. J. 438 (2022) 135655.
[39] J. Zhao, Y. He, J. Wang, M. Peng, J. Yang, F. Zeng, Effect of in-situ emulsification on CO_2/N_2-based cyclic solvent injection process for enhancing heavy oil recovery and CO_2 storage, Chem. Eng. Sci. 295 (2024) 120185.
[40] C.A. Carrillo, D. Saloni, L.A. Lucia, M.A. Hubbe, O.J. Rojas, Capillary flooding of wood with microemulsions from Winsor I systems, J. Colloid Interface Sci. 381 (1) (2012) 171–179.
[41] J. Wang, Y. Sun, M. Yu, X. Lu, S. Komarneni, C. Yang, Emulsions stabilized by highly hydrophilic TiO2 nanoparticles via van der Waals attraction, J. Colloid Interface Sci. 589 (2021) 378–387.
[42] M. Koroleva, D. Bidanov, E. Yurtov, Emulsions stabilized with mixed SiO 2 and Fe 3 O 4 nanoparticles: mechanisms of stabilization and long-term stability, Phys. Chem. Chem. Phys. 21 (3) (2019) 1536–1545.
[43] Z. Sun, X. Yan, Y. Xiao, L. Hu, M. Eggersdorfer, D. Chen, Z. Yang, D.A. Weitz, Pickering emulsions stabilized by colloidal surfactants: role of solid particles, Particuology 64 (2022) 153–163.
[44] P.A. Kralchevsky, I.B. Ivanov, K.P. Ananthapadmanabhan, A. Lips, On the thermodynamics of particle-stabilized emulsions: curvature effects and catastrophic phase inversion, Langmuir 21 (1) (2005) 50–63.
[45] B.P. Binks, S.O. Lumsdon, Pickering emulsions stabilized by monodisperse latex particles: effects of particle size, Langmuir 17 (15) (2001) 4540–4547.
[46] A. Einstein, On the motion of small particles suspended in liquids at rest required by the molecular-kinetic theory of heat, Ann. Phys. 17 (7) (1905) 208.
[47] R. Khoramian, R. Kharrat, P. Pourafshary, S. Golshokooh, F. Hashemi, Spontaneous imbibition oil recovery by natural surfactant/nanofluid: an experimental and theoretical study, Nanomaterials 12 (20) (2022) 3563.
[48] Q. Zhou, W. Wang, Z. Jiang, Y. Cao, J. Xiao, Enhancing stability of Pickering emulsions: insights into the interfacial dynamics of Zein-MCT composite nanoparticles, Food Hydrocoll. 148 (2024) 109504.
[49] X. Feng, H. Dai, L. Ma, Y. Fu, Y. Yu, H. Zhou, T. Guo, H. Zhu, H. Wang, Y. Zhang, Properties of Pickering emulsion stabilized by food-grade gelatin nanoparticles: influence of the nanoparticles concentration, Colloids Surf. B Biointerfaces 196 (2020) 111294.
[50] J.A. Juárez, C.P. Whitby, Oil-in-water Pickering emulsion destabilisation at low particle concentrations, J. Colloid Interface Sci. 368 (1) (2012) 319–325.
[51] B. Madivala, J. Fransaer, J. Vermant, Self-assembly and rheology of ellipsoidal particles at interfaces, Langmuir 25 (5) (2009) 2718–2728.
[52] I. Kalashnikova, H. Bizot, B. Cathala, I. Capron, New Pickering emulsions stabilized by bacterial cellulose nanocrystals, Langmuir 27 (12) (2011) 7471–7479.
[53] E. Hosseini, F. Hajivand, A. Yaghodous, R. Soltani, Experimental investigation of the effect of dispersed silica and alumina nanoparticles on oil-aqueous phase interfacial tension, Pet. Sci. Technol. 37 (13) (2019) 1485–1494.
[54] S. Golshokooh, S.A. Ramazani, A. and Hekmatzadeh, M., Investigating the effect of hybrid silica nanoparticles-copolymer on increasing oil recovery in a three-dimensional porous media, Scientia Iranica 24 (6) (2017) 3466–3475.
[55] Z. Wang, H. Jia, X. Geng, S. Wen, X. Zhang, X. Wen, Q. Xie, P. Huang, Synthesis of thiol and dodecyl functionalized silica nanoparticles to stabilize Pickering emulsion for enhanced oil recovery, J. Mol. Liq. 427 (2025) 127439.
[56] L. Xu, S. Wen, Q. Xie, F. Fan, Q. Wang, X. Zhang, K. Lv, H. Jia, H. Sun, Interfacial rheological investigation of modified silica nanoparticles with different alkyl chain lengths at the n-octane/water interface, Molecules 29 (16) (2024) 3749.
[57] J. Smits, R.P. Giri, C. Shen, D. Mendonça, B. Murphy, P. Huber, K. Rezwan, M. Maas, Synergistic and competitive adsorption of hydrophilic nanoparticles and oil-soluble surfactants at the oil–water interface, Langmuir 37 (18) (2021) 5659–5672.
[58] N. Briggs, A.K.Y. Raman, L. Barrett, C. Brown, B. Li, D. Leavitt, C.P. Aichele, S. Crossley, Stable Pickering emulsions using multi-walled carbon nanotubes of varying wettability, Colloids Surf. A Physicochem. Eng. Asp. 537 (2018) 227–235.
[59] R.N. Wenzel, Surface roughness and contact angle, J. Phys. Chem. 53 (9) (1949) 1466–1467.
[60] D. Joshi, N.K. Maurya, A. Mandal, Experimental studies on effectiveness of graphene oxide nanosheets dispersion in water/aqueous PHPA for enhanced oil recovery, J. Mol. Liq. 387 (2023) 122728.
[61] K. Ono, Disjoining pressure derived from the Lennard–Jones potential, diffusion equation, and diffusion coefficient for submonolayer liquid film, Surfaces 1 (1) (2018) 122–137.
[62] V. Valmacco, M. Elzbieciak-Wodka, C. Besnard, P. Maroni, G. Trefalt, M. Borkovec, Dispersion forces acting between silica particles across water: influence of nanoscale roughness, Nanoscale Horizons 1 (4) (2016) 325–330.
[63] Q. Khan, P. Pourafshary, F. Hadavimoghaddam, R. Khoramian, Machine learning prediction of CO_2 diffusion in brine: model development and salinity influence under reservoir conditions, Appl. Sci. 15 (15) (2025) 8536.
[64] R. Khoramian, P. Pourafshary, M. Riazi, The role of capillary hysteresis in enhancing CO_2 trapping efficiency and storage stability, Kazakhstan Journal for Oil & Gas Industry 7 (1) (2025) 90–99.
[65] R. Khoramian, I. Salaudeen, P. Pourafshary, M. Riazi, R. Kharrat, Impact of relative permeability hysteresis on CO_2 storage in saline aquifers, Greenhouse Gases: Science and Technology 15 (1) (2025) 3–12.